

# Crossing of large multi-quasiparticle magnetic rotation bands in $^{198}\text{Bi}$

H. Pai,\* G. Mukherjee,† S. Bhattacharya, C. Bhattacharya, S. Bhattacharyya, T. Bhattacharjee, S. K. Basu, S. Kundu, T. K. Ghosh, K. Banerjee, T. K. Rana, and J. K. Meena  
*Variable Energy Cyclotron Centre, Kolkata 700064, India*

R. K. Bhowmik, R.P. Singh, S. Muralithar  
*Inter University Accelerator Centre, Aruna Asaf Ali Marg, New Delhi 110067, INDIA*

S. Chanda  
*Fakir Chand College, Diamond Harbour, West Bengal, India*

R. Garg  
*Department of Physics and Astrophysics, University of Delhi, New Delhi, INDIA*

B. Maheshwari and A. K. Jain  
*Department of Physics, Indian Institute of Technology, Roorkee-247667, India*  
 (Dated: December 18, 2018)

High-spin states in the doubly-odd  $^{198}\text{Bi}$  nucleus have been studied by using the  $^{185,187}\text{Re}(^{16}\text{O}, \text{xn})$  reactions at the beam energy of 112.5 MeV.  $\gamma-\gamma$  coincidence were measured by using the INGA array with 15 Compton suppressed clover HPGe detectors. The observed levels have been assigned definite spin-parity. The high spin structure is grouped into three bands (B1, B2 and B3), of which two (B1 and B2) exhibit the properties of magnetic rotation (MR). Tilted axis cranking calculations were carried out to explain the MR bands having large multi-quasiparticle configurations. The calculated results explain the bands B1 and B2 very nicely, confirming the shears mechanism and suggest a crossing of two MR bands in both the cases. The crossing is from 6-qp to 8-qp in band B1 and from 4-qp to 6-qp in band B2, a very rare finding. A semiclassical model has also been used to obtain the particle-hole interaction strengths for the bands B1 and B2, below the band crossing.

PACS numbers: 21.10.Re; 23.20.Lv; 23.20.En; 27.80.+w

## I. INTRODUCTION

The ‘‘Magnetic rotation (MR)’’, is an interesting phenomena where the rotation of a ‘‘magnetic top’’ is involved. Right conditions for such a rotation arise in weakly deformed configurations where neutron (proton) particles and proton (neutron) holes in high- $j$  orbitals are coupled to each other [1, 2]. These MR bands were observed in significant numbers in the mass region  $A \sim 190$  and  $Z \sim 82$  [3], where the proton shell closure ensures a nearly spherical shape. The high- $j$  proton particles in the  $h_{9/2}$  and  $i_{13/2}$  orbitals and neutron holes in the  $i_{13/2}$  orbital play important roles in the Pb, Bi and Tl isotopes, where many good examples of MR bands were found [4–10]. However, the configuration assignments in many cases remains uncertain due to incomplete knowledge of the spin-parity of the bands [9, 10].

In the present work, we investigate the high-spin states in  $^{198}\text{Bi}$ , where only a limited information about the high spin states is known. Apart from the ground state ( $T_{1/2} = 10.3$  min), only two other low-lying isomeric states were known until recently. Among these, the ( $7^+$ ) level ( $T_{1/2} = 11.6$  min) decays by  $\beta$ -decay and no  $\gamma$ -transition from this level is known. Therefore, the excitation energy of this state remains unknown. A  $10^-$  isomeric state was reported by Hagemann et al. [11] in 1972 at an excitation energy of 248 keV with respect to the 11.6-min isomeric state. This state was interpreted as a member of the  $|\nu i_{13/2}^{-1} \otimes \pi h_{9/2}; J\rangle$  multiplet. More recently, excited states in  $^{198}\text{Bi}$  were studied by Zhou et al. [12] through  $\gamma$ -ray spectroscopy following  $^{187}\text{Re}(^{16}\text{O}, 5n)$  reaction using six Compton suppressed HPGe detectors. The  $\gamma$  rays above the  $10^-$  isomer in this nucleus were assigned from the  $\gamma$ -ray excitation functions and a level scheme was proposed by them from the  $\gamma$ - $\gamma$  coincidence measurements. In this measurement, spins and parities were assigned only for a few states and the level scheme was known upto  $\sim 4$  MeV. The higher lying states in  $^{198}\text{Bi}$  have been interpreted by considering the coupling of the  $h_{9/2}$  proton with the high-spin states observed in  $^{197}\text{Pb}$  above its  $13/2^+$

\*Present Address: Institut für Kernphysik, Technische Universität Darmstadt, GERMANY; Electronic address: hari.vecc@gmail.com, hpai@ikp.tu-darmstadt.de, H.Pai@gsi.de  
 †Corresponding author; Electronic address: gopal@vecc.gov.in

isomeric state. Later on, Zwartz et al. [9] proposed three unconnected MR-type bands in  $^{198}\text{Bi}$ , namely Band 1, Band 2 and Band 3 from the measurement of B(M1)/B(E2) ratios. In their experiment the  $\gamma$ -ray transitions were assigned in  $^{198}\text{Bi}$  by examining associated BGO calorimeter energy spectrum. However, neither the spin-parity ( $J^\pi$ ) nor the excitation energies of the states were known and hence, the configuration of these bands also remained uncertain.

In the present work, we have carried out a detailed  $\gamma$ -ray spectroscopy of  $^{198}\text{Bi}$  upto high spins and established the spin-parity of the excited states. This enables us to identify three band like structures B1, B2 and B3, of which two (B1 and B2) are proposed as MR bands. We assign definite configurations to both these bands. We further showed that each of the two bands (B1 and B2) represents a crossing of two large multi- quasiparticle configuration bands. In B1, the crossing is between a 6-qp and a 8-qp MR band, whereas in B2, the crossing is between a 4-qp and a 6-qp MR band, something very rarely observed.

## II. EXPERIMENTAL METHOD AND THE LEVEL SCHEME

The  $\gamma$ -ray spectroscopy of  $^{198}\text{Bi}$  has been studied at 15-UD Pelletron at IUAC, New Delhi, India using the Indian National Gamma Array (INGA) [13] with 15 Compton suppressed clover detectors at the time of the experiment. The excited states of odd-odd  $^{198}\text{Bi}$  were populated by fusion evaporation reactions  $^{185,187}\text{Re}(^{16}\text{O}, xn)^{198}\text{Bi}$  at 112.5 MeV of beam energy. The target was a thick ( $18.5 \text{ mg/cm}^2$ ) natural rhenium foil. The recoils were stopped inside the target itself. The isotopic ratio of  $^{185}\text{Re}$  and  $^{187}\text{Re}$  in the natural rhenium is 37:63. The clover detectors were arranged in five angles with respect to the beam direction having four clovers each at  $90^\circ$  and  $148^\circ$ , two clovers each at  $123^\circ$  and  $57^\circ$  and three clovers at  $32^\circ$  angles. List mode data were recorded using  $\gamma$ - $\gamma$ - $\gamma$  trigger. About  $2.4 \times 10^8$  coincidence events were recorded in this experiment.  $E_\gamma$ - $E_\gamma$  matrix and  $E_\gamma$ - $E_\gamma$ - $E_\gamma$  cubes were constructed from the collected coincidence data. To construct these, a coincidence window of  $\pm 400$  ns was selected. The matrix was primarily used for the subsequent analysis. The RADWARE software [14] was used for the analysis of the matrix and the cube. The clover detectors were calibrated for  $\gamma$ -ray energies and efficiencies by using  $^{133}\text{Ba}$  and  $^{152}\text{Eu}$  radioactive sources.

The multiplicities of the  $\gamma$ -ray transitions have been determined from the angular correlation analysis using the method of directional correlation from the oriented states (DCO) ratio, following the prescriptions of Krämer-Flecken et al. [15]. For the

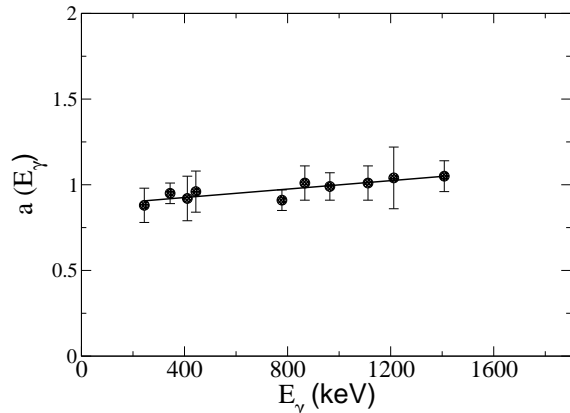


FIG. 1: The asymmetry correction factor  $a(E_\gamma)$  at different  $\gamma$  energies from  $^{152}\text{Eu}$  source. The solid line corresponds to a linear fit of the data.

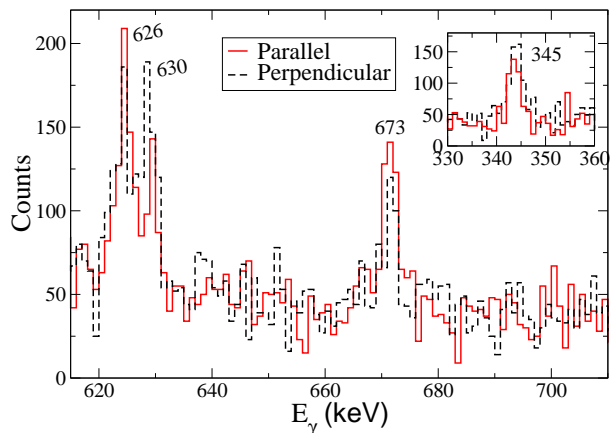


FIG. 2: (Color online) The perpendicular (dashed black coloured) and parallel (solid red coloured) components of 626-, 630- and 673-keV  $\gamma$  rays in  $^{198}\text{Bi}$ , obtained from the IPDCO analysis in the present work. The same for the 345-keV  $\gamma$  ray is shown in the inset.

DCO ratio analysis, the coincidence events were sorted into an asymmetry matrix with data from the  $90^\circ$  detectors ( $\theta_1$ ) on one axis and  $148^\circ$  detectors ( $\theta_2$ ) on the other axis. The DCO ratios (for  $\gamma_1$ , gated by a  $\gamma$  ray  $\gamma_2$  of known multipolarity) are obtained from the intensities of the  $\gamma$  rays ( $I_\gamma$ ) at two angles  $\theta_1$  and  $\theta_2$ , as

$$R_{DCO} = \frac{I_{\gamma_1} \text{ at } \theta_1, \text{ gated by } \gamma_2 \text{ at } \theta_2}{I_{\gamma_1} \text{ at } \theta_2 \text{ gated by } \gamma_2 \text{ at } \theta_1} \quad (1)$$

By putting gates on the transitions with known multipolarity along the two axes of the above matrix, the DCO ratios are obtained for each  $\gamma$  ray. For stretched transitions, the value of  $R_{DCO}$  would be close to unity for the same multipolarity of  $\gamma_1$  and

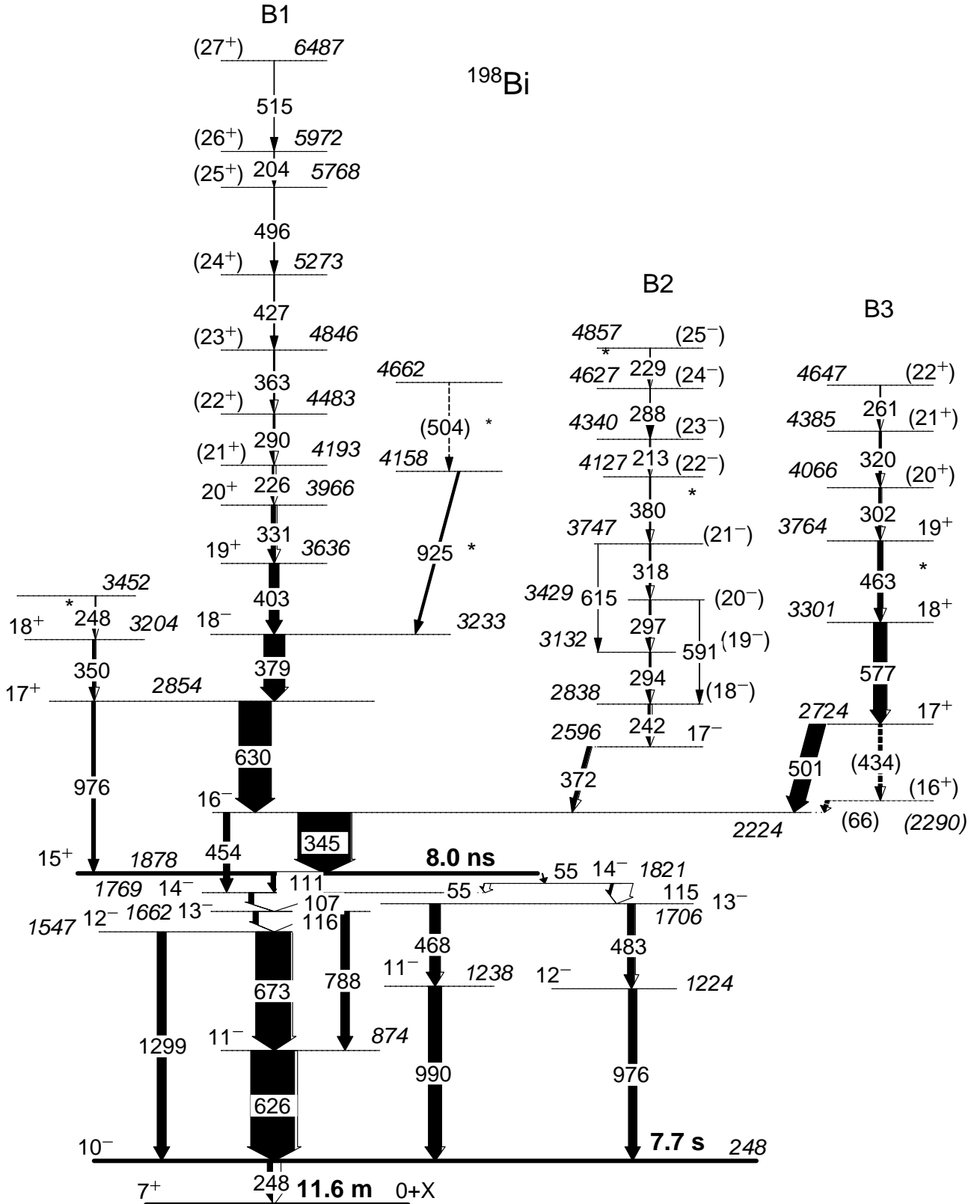


FIG. 3: Level scheme of  $^{198}\text{Bi}$  as proposed from this work. The excitation energy of the 11.6 m isomer is not known so it has been put as  $0+X$ . The excitation energy of all other transitions are given in reference to this isomer. The new  $\gamma$  rays are indicated by \*.

$\gamma_2$ . For different multiplicities and mixed transition, the value of  $R_{DCO}$  depends on the detector angles ( $\theta_1$  and  $\theta_2$ ) and the mixing ratio ( $\delta$ ). The validity of the  $R_{DCO}$  measurements was checked with the known transitions in  $^{198}\text{Bi}$  and with the calculated values. In the present geometry, the calculated value of  $R_{DCO}$  [16] for a pure dipole transition gated by a stretched quadrupole transition is 1.81 while for a quadrupole transition gated by a pure dipole, the calculated value is 0.55. These compare well with the experimental values of 1.81(27) and 0.53(10), respectively, for the known dipole (345.5-keV,  $E1$ ) and quadrupole (468.2-keV,  $E2$ ) transitions.

Definite parities of the excited states have been assigned from the integrated polarization asymmetry (IPDCO) ratio, as described in Ref. [8, 17–19], from the parallel and perpendicular scattering of a  $\gamma$ -ray photon inside the detector medium. The IPDCO ratio measurement gives a qualitative idea about the type of the transitions ( $E/M$ ). The IPDCO asymmetry parameters have been deduced using the relation,

$$\Delta_{IPDCO} = \frac{a(E_\gamma)N_\perp - N_\parallel}{a(E_\gamma)N_\perp + N_\parallel}, \quad (2)$$

where  $N_\parallel$  and  $N_\perp$  are the counts for the actual Compton scattered  $\gamma$  rays in the planes parallel and perpendicular to the reaction plane. The correction due to the asymmetry in the array and response of the clover segments, defined by  $a(E_\gamma) = \frac{N_\parallel}{N_\perp}$ , was checked using  $^{152}\text{Eu}$  source. The values of  $a(E_\gamma)$

have been obtained using the expression  $a(E_\gamma) = a + b(E_\gamma)$ . The fitting, shown in Fig. 1, gives the values of the constants as  $a = 0.88(2)$  and  $b(E_\gamma) = 0.00012(3)$ . A positive value of  $\Delta_{IPDCO}$  indicates an electric type transition whereas a negative value indicates a magnetic type transition. The low energy cut off for the polarization measurement was about 200 keV, in the present work.

The polarization method was verified from the  $\gamma$  rays of known electric or magnetic character. Sum gated spectra have been used for polarization measurement in the present work. The parallel ( $N_\parallel$ ) and perpendicular ( $a(E_\gamma)N_\perp$ ) counts for the  $\gamma$  rays in  $^{198}\text{Bi}$  are shown in Fig. 2. The 626- and 673-keV  $\gamma$  ray were known to decay from  $11^-$  state to  $10^-$  state and from  $12^-$  to  $11^-$  state, respectively [12]. These transitions were known as mixed  $M1 + E2$  transitions. It can be clearly seen that the counts in the parallel scattered components are more in these two peaks than the perpendicular ones. However, for the 345- and 630-keV  $\gamma$  rays, the situation is found to be opposite. The IPDCO ratio for several other transitions has also been obtained in this work and together with the DCO ratio measurements, firm spin-parity assignment could be done for several states.

An improved level scheme, of  $^{198}\text{Bi}$  obtained in this work, is given in Fig. 3. The deduced excitation energy, spin and parity of the excited levels and the multipolarity of the  $\gamma$  rays, together with other relevant information concerning their placement in the proposed level scheme, are summarized in Table I.

TABLE I: Energies ( $E_\gamma$ ), intensities ( $I_\gamma$ ), DCO ratios ( $R_{DCO}$ ), IPDCO ratios ( $\Delta_{IPDCO}$ ) and deduced multiplicities of the  $\gamma$  rays in  $^{198}\text{Bi}$ . The energies of initial states ( $E_i$ ) and spins and parities of initial ( $J_i^\pi$ ) and final ( $J_f^\pi$ ) states are also given.

$E_\gamma$ (in keV)	$E_i$ (in keV)	$J_i^\pi \rightarrow J_f^\pi$	$I_\gamma$ [1]	$R_{DCO}$ (Err)	$\Delta_{IPDCO}$ (Err)	Deduced Multipolarity
(66)	(2290)	$(16^+) \rightarrow 16^-$	-	-	-	(E1)
106.6(2)	1769.0	$14^- \rightarrow 13^-$	9.6(12)	0.91(24) <sup>[4]</sup>	-	M1+E2
110.8(4)	1878.2	$15^+ \rightarrow 14^-$	8.6(11)	0.98(26) <sup>[2]</sup>	-	E1
115.2(3)	1821.5	$14^- \rightarrow 13^-$	5.1(7)	1.69(46) <sup>[3]</sup>	-	M1+E2
115.8(2)	1662.4	$13^- \rightarrow 12^-$	10.0(12)	1.05(25) <sup>[4]</sup>	-	M1+E2
203.5(3)	5971.3	$(26^+) \rightarrow (25^+)$	1.0(2)	-	-	(M1) <sup>[5]</sup>
212.9(2)	4339.7	$(23^-) \rightarrow (22^-)$	1.1(2)	-	-	(M1) <sup>[5]</sup>
226.2(6)	4192.5	$(21^+) \rightarrow 20^+$	3.0(4)	-	-	(M1) <sup>[5]</sup>
229.2(1)	4856.7	$(25^-) \rightarrow (24^-)$	0.6(1)	-	-	(M1)
242.2(2)	2838.2	$(18^-) \rightarrow 17^-$	4.3(5)	-	-	(M1) <sup>[5]</sup>
248.3(3)	3452.2	-	0.8(1)	-	-	-
261.2(4)	4646.6	$(22^+) \rightarrow (21^+)$	1.1(2)	-	-	(M1) <sup>[5]</sup>
287.8(3)	4627.5	$(24^-) \rightarrow (23^-)$	0.8(1)	-	-	(M1) <sup>[5]</sup>
290.3(2)	4482.8	$(22^+) \rightarrow (21^+)$	1.6(2)	-	-	(M1) <sup>[5]</sup>
294.1(3)	3132.3	$(19^-) \rightarrow (18^-)$	2.8(3)	-	-	(M1) <sup>[5]</sup>
296.6(3)	3429.3	$(20^-) \rightarrow (19^-)$	2.4(3)	-	-	(M1) <sup>[5]</sup>
301.8(3)	4065.5	$(20^+) \rightarrow 19^+$	4.2(6)	-	-	(M1) <sup>[5]</sup>
317.5(3)	3747.0	$(21^-) \rightarrow (20^-)$	2.1(3)	-	-	(M1) <sup>[5]</sup>

Table I: Continued...

$E_\gamma$ (in keV)	$E_i$ (in keV)	$J_i^\pi \rightarrow J_f^\pi$	$I_\gamma$ [1]	$R_{DCO}$ (Err)	$\Delta_{IPDCO}$ (Err)	Deduced Multipolarity
319.8(4)	4385.3	(21 <sup>+</sup> ) $\rightarrow$ (20 <sup>+</sup> )	3.2(5)	-	-	(M1) <sup>[5]</sup>
330.6(2)	3966.3	20 <sup>+</sup> $\rightarrow$ 19 <sup>+</sup>	8.2(10)	1.01(20) <sup>[6]</sup>	-0.25(10)	M1
345.5(1)	2223.6	16 <sup>-</sup> $\rightarrow$ 15 <sup>+</sup>	100.0(30)	1.81(27) <sup>[3]</sup>	0.18(5)	E1
349.9(4)	3204	18 <sup>+</sup> $\rightarrow$ 17 <sup>+</sup>	5.0(4)	0.94(26) <sup>[2]</sup>	-	M1+E2
362.9(3)	4845.7	(23 <sup>+</sup> ) $\rightarrow$ (22 <sup>+</sup> )	1.6(2)	-	-	(M1) <sup>[5]</sup>
372.4(2)	2596.0	17 <sup>-</sup> $\rightarrow$ 16 <sup>-</sup>	7.2(6)	0.96(17) <sup>[2]</sup>	-0.26(15)	M1
379.1(1)	3233.2	18 <sup>-</sup> $\rightarrow$ 17 <sup>+</sup>	39.0(20)	1.80(30) <sup>[3]</sup>	0.16(7)	E1
379.8(1)	4126.8	(22 <sup>-</sup> ) $\rightarrow$ (21 <sup>-</sup> )	1.8(2)	-	-	(M1)
402.6(4)	3635.8	19 <sup>+</sup> $\rightarrow$ 18 <sup>-</sup>	18.3(12)	0.91(10) <sup>[6]</sup>	0.16(7)	E1
426.5(3)	5272.2	(24 <sup>+</sup> ) $\rightarrow$ (23 <sup>+</sup> )	1.3(2)	-	-	(M1) <sup>[5]</sup>
(434)	2724.4	17 <sup>+</sup> $\rightarrow$ (16 <sup>+</sup> )	6(1)	-	-	(M1)
453.7(3)	2223.6	16 <sup>-</sup> $\rightarrow$ 14 <sup>-</sup>	11.4(7)	0.61(12) <sup>[4]</sup>	0.23(8)	E2
462.5(2)	3763.7	19 <sup>+</sup> $\rightarrow$ 18 <sup>+</sup>	8.90(7)	0.98(19) <sup>[2]</sup>	-	M1
468.2(1)	1706.3	13 <sup>-</sup> $\rightarrow$ 11 <sup>-</sup>	19.8(10)	0.53(10) <sup>[2]</sup>	0.21(6)	E2
483.4(1)	1706.3	13 <sup>-</sup> $\rightarrow$ 12 <sup>-</sup>	13.0(12)	1.01(25) <sup>[2]</sup>	-0.26(10)	M1+E2
495.5(4)	5767.8	(25 <sup>+</sup> ) $\rightarrow$ (24 <sup>+</sup> )	1.2(2)	-	-	(M1) <sup>[5]</sup>
500.8(1)	2724.4	17 <sup>+</sup> $\rightarrow$ 16 <sup>-</sup>	30.4(15)	0.97(11) <sup>[2]</sup>	0.20(11)	E1
504	4662	-	1.0(1)	-	-	-
515.1(5)	6486.4	(27 <sup>+</sup> ) $\rightarrow$ (26 <sup>+</sup> )	0.8(2)	-	-	(M1) <sup>[5]</sup>
576.7(1)	3301.2	18 <sup>+</sup> $\rightarrow$ 17 <sup>+</sup>	23.7(15)	1.04(26) <sup>[2]</sup>	-0.25(10)	M1
591.3(3)	3429.3	(20 <sup>-</sup> ) $\rightarrow$ (18 <sup>-</sup> )	0.5(1)	-	-	(E2) <sup>[5]</sup>
615.2(5)	3747.0	(21 <sup>-</sup> ) $\rightarrow$ (19 <sup>-</sup> )	0.6(1)	-	-	(E2) <sup>[5]</sup>
625.8(1)	873.8	11 <sup>-</sup> $\rightarrow$ 10 <sup>-</sup>	82.9(29)	1.07(16) <sup>[2]</sup>	-0.14(6)	M1(+E2)
630.5(1)	2854.1	17 <sup>+</sup> $\rightarrow$ 16 <sup>-</sup>	61.1(25)	0.99(10) <sup>[2]</sup>	0.21(7)	E1
672.8(1)	1546.6	12 <sup>-</sup> $\rightarrow$ 11 <sup>-</sup>	66.0(24)	0.84(12) <sup>[2]</sup>	-0.24(6)	M1+E2
787.5(1)	1662.4	13 <sup>-</sup> $\rightarrow$ 11 <sup>-</sup>	16.2(11)	0.60(10) <sup>[2]</sup>	0.19(8)	E2
924.8(2)	4158.0	-	4.3(6)	-	-	-
975.9(2)	1223.8	12 <sup>-</sup> $\rightarrow$ 10 <sup>-</sup>	16.0(12)	0.54(11) <sup>[2]</sup>	0.13(7)	E2
976.4(3)	2854.1	17 <sup>+</sup> $\rightarrow$ 15 <sup>+</sup>	7.1(6)	0.65(18) <sup>[4]</sup>	-	E2
990.1(2)	1238.1	11 <sup>-</sup> $\rightarrow$ 10 <sup>-</sup>	24.6(10)	1.61(29) <sup>[2]</sup>	-0.12(8)	M1+E2
1298.7(2)	1546.6	12 <sup>-</sup> $\rightarrow$ 10 <sup>-</sup>	17.0(8)	0.62(14) <sup>[2]</sup>	0.12(8)	E2

Representative single gated  $\gamma$ -ray spectra are shown in Figs. 4(a) and Fig. 4(b). These spectra show the known  $\gamma$  lines corresponding to the low-lying transitions and the  $\gamma$ -lines (242-, 297-, 318-, 226-, 331-, 501- and 577-keV) belonging to the proposed MR bands. The other weaker  $\gamma$  lines were observed in the sum-gated spectra which have been

discussed later on. The 55-keV  $\gamma$ -ray doublet, reported by Zhou et al. [12], could not be observed as the energy threshold was somewhat more than 55 keV in the present experiment. The 223-keV  $\gamma$  ray, reported in [12], is not observed in the present data. So, it was not placed in the level scheme shown in Fig. 3.

The spin and parity of the levels up to the 1662 keV were assigned by Zhou et al. from their angular distribution measurements. The 107-keV transition, placed above the 1662 keV level, has been assigned as mixed (M1+E2) transition in this work and, hence, the spin-parity ( $J^\pi$ ) of 14<sup>-</sup> has been assigned for the 1769-keV level. The  $J^\pi$  assignment of the 2224-keV level is crucial for the assignment of  $J^\pi$  and, hence, the configuration of the bands built on top of that level. In the previous work, the  $J^\pi$  of this level was tentatively assigned as (16<sup>+</sup>). This was based on the fact that 345- and 454-keV transitions were found to be dipole and quadrupole in nature from the angular distribution measurement in ref. [12]. It was also assumed, without polariza-

[1] Relative  $\gamma$  ray intensities are estimated from prompt spectra and normalized to 100 for the total intensity of 345.5-keV  $\gamma$  rays.

[2] From 345.5 keV (E1) DCO gate;

[3] From 975.9 keV (E2) DCO gate;

[4] From 625.8 keV (M1(+E2)) DCO gate;

[5] Adopted from ref. [9];

[6] From 379.1 keV (E1) DCO gate;

[7] From 468.2 keV (E2) DCO gate;

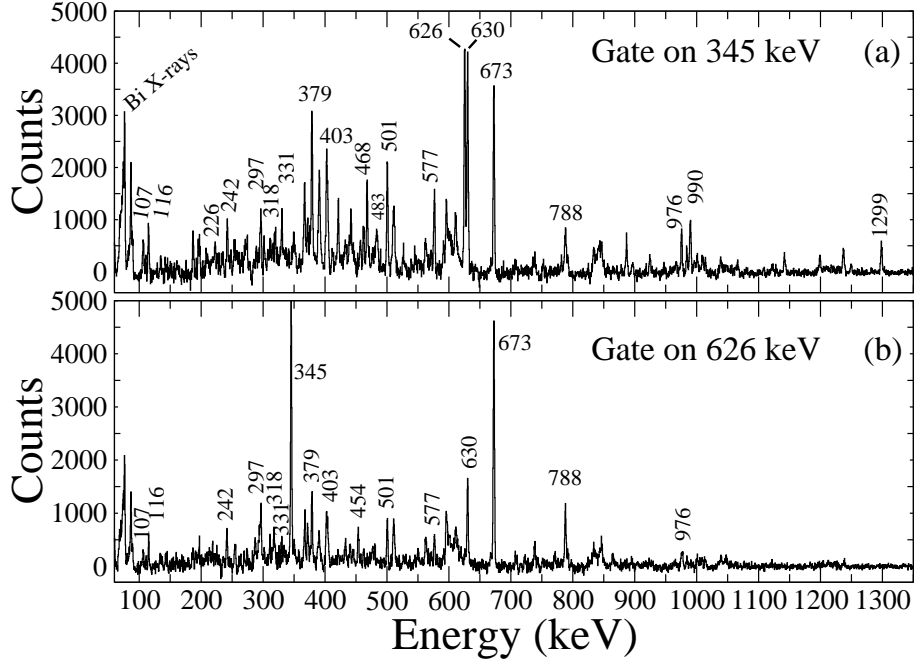


FIG. 4: Single gated spectra of  $^{198}\text{Bi}$  gated by 345-keV (a) and 626-keV (b) transitions. The marked peaks belong to  $^{198}\text{Bi}$ .

tion measurement, that the 345-keV  $\gamma$  ray is a mixed  $M1 + E2$  transition. If this was the case, then the 455-keV  $\gamma$  ray turns out to be a  $M2$  transition, although no evidence for a longer half-life corresponding to such a transition was obtained for the 2224-keV level.

In the present work, the DCO ratio measurement of the 345- and the 454-keV  $\gamma$  rays indicate that they are indeed dipole and quadrupole in nature. The polarization measurement of the 345-keV  $\gamma$  ray is shown in Fig 2 (inset); which clearly shows that the perpendicular counts are more than the parallel counts. The  $\Delta_{IPDCO}$  value obtained for this transition suggests that it is electric type. Hence, 345-keV  $\gamma$  ray is an  $E1$  transition. Therefore, the  $J^\pi = 16^-$  is assigned for the 2224-keV level. This assignment is well supported by the  $E2$  assignment of the 454-keV  $\gamma$  ray from its DCO ratio and  $\Delta_{IPDCO}$  values. The three transitions above this 2224 keV state, namely 630, 379 and 403 keV have been found to be of  $E1$  type. The previous angular distribution measurements [12] and our DCO ratio measurement agrees to assign dipole character for these transitions. The polarization measurements in our work show positive value of  $\Delta_{IPDCO}$  for these transitions as shown in Fig.2 for 630-keV  $\gamma$  ray. Therefore, the  $J^\pi$  of the levels at 2854, 3233 and 3636 keV are assigned as  $17^+$ ,  $18^-$  and  $19^+$ , respectively. These assignments are also supported by the observed quadrupole nature of the 976-keV transition. The other two tran-

sitions above the 2224 keV  $16^-$  state, namely 372- and 501-keV, have been found to be of  $M1$  and  $E1$  types from their negative and positive  $\Delta_{IPDCO}$  values, respectively. Therefore, the parity of the bands B2 and B3 have opposite parity.

The DCO ratios of the transitions belonging to the MR bands as reported by Zwartz et al [9] could not be measured in the present work due to their low intensities except for a few transitions which lie towards the bottom of the bands. These few transitions supported the assignment of Ref. [9]. So, the multipolarity of the transitions in these bands were adopted from Zwartz et al and are presented in Table-I.

Fig. 5 shows three different sum coincidence spectra which were generated with suitable sum gate on several in-band transitions of previously known [9] three MR bands B1 (Fig. 5(a)) B2 (Fig. 5(b)) and B3 (Fig. 5(c)). The peaks marked by \* and + in these spectra belong to the MR bands and the previously known lower-lying transitions [12] in  $^{198}\text{Bi}$ , respectively. The sum gated spectrum of 204-, 226- and 427-keV from band B1 clearly shows all the transitions of previously known MR band along with the known lower-lying transitions in  $^{198}\text{Bi}$ . In this spectrum  $\gamma$  lines belong to other two MR bands B2 and B3 were not observed but the lower-lying transitions 331-, 403-, 379-, 345-, 673-, 626-keV and other transitions of  $^{198}\text{Bi}$  have been observed. Therefore, we have placed MR band B1 above the 3636-keV state.

On the other hand, the sum gated spectrum of 242-, 297- and 372-keV shows all transitions of the band B2 along with the known lower-lying  $\gamma$  lines in  $^{198}\text{Bi}$ . In this spectrum transitions of other two bands B1 and B3 were not observed. The 345-, 673-, 626- keV lines and other  $\gamma$  lines of  $^{198}\text{Bi}$  have been observed in this spectrum. However, the transitions at 331, 403, 350 and 630 keV are absent in this spectrum. Therefore, the band B2 has been placed on top of the 2596 keV level.

Two cross-over E2 transitions have been observed in band B2: the 615-keV (from the 3747 keV level)  $\gamma$  ray between the 318- and 297-keV M1 transitions; and the 591 keV (from 3429 keV level)  $\gamma$  ray between the 297- and 294-keV M1 transitions. B(M1)/B(E2) ratios for these two levels have been found to be 6.6 (14) and 9.2 (21)  $\mu^2/(eb)^2$ , respectively, which agrees well with the values reported by Zwartz et al. [9].

The sum gated spectrum of 577-keV and 302-keV (Fig. 5(c)) shows all the  $\gamma$  lines of the band B3 along with the known lower-lying  $\gamma$  lines in  $^{198}\text{Bi}$ . In this spectrum, transitions of other two bands B1 and B2 have not been observed. Known  $\gamma$  lines at 331, 403, 379, 350 and 630 keV were not observed in this spectrum. However, 345-, 673-, 626-keV and other known lower-lying transitions in  $^{198}\text{Bi}$  have been identified. Therefore, we have placed band B3 on top of the 2224-keV state. A strong 501-keV line has also been observed in this spectrum which connects the band B3 with the  $16^-$  level. There is an indication of a weak 434-keV line in the spectrum. When we gate on this 434-keV  $\gamma$  peak, the strong lines at 577 and 463 keV are observed along with some of the low-lying known transitions but the 501-keV line was not observed. Also, the 434-keV line can be seen, albeit small intensity, in 577-keV gate but is not present in the 501-keV gate. Therefore, we believe that the 2724-keV level decays to a tentatively assigned  $16^+$  level at 2290 keV via this 434 keV tentative transition which is the most likely band-head of the band B3.

### III. RESULTS AND DISCUSSION

The low-lying states in the odd-odd nuclei are generated by the coupling of the odd-proton and odd-neutron in the valence orbitals near the Fermi energy. The  $h_{9/2}$ ,  $i_{13/2}$  and  $s_{1/2}$  proton orbitals and  $i_{13/2}$ ,  $f_{5/2}$  and  $p_{3/2}$  neutron orbitals are available in  $^{198}\text{Bi}$ , which is weakly oblate in nature. As an example, the  $2^+$  and  $7^+$  states are generated by parallel and anti-parallel particle-hole couplings of  $\pi h_{9/2} \otimes \nu f_{5/2}^{-1}$  orbitals. Similarly, the low-lying  $10^-$  isomer observed in the odd-odd nuclei in this region, has the configuration of  $\pi h_{9/2} \otimes \nu i_{13/2}^{-1}$ . We may generate the higher-lying states coupling

these configurations with the two-proton or, two-neutron configurations coming from the breaking of a proton pair or, a neutron pair. For example, the important two-neutron negative parity configurations are,  $5^-$  ( $\nu i_{13/2}^{-1} p_{3/2}^{-1}$ ) and  $9^-$  ( $\nu i_{13/2}^{-1} f_{5/2}^{-1}$ ). Similarly, the important proton configurations available are  $8^+$  ( $\pi h_{9/2}^2 s_{1/2}^{-2}$ ),  $5^-$  ( $\pi h_{9/2} s_{1/2}$ ) and  $11^-$  ( $\pi h_{9/2} i_{13/2} s_{1/2}^{-2}$ ), which are observed in the even-even Pb isotopes. Infact, the highest-j orbital is the  $\nu i_{13/2}$  orbital, which is expected to play a crucial role in most of the multi-qp configurations.

The  $15^+$  isomer in  $^{198}\text{Bi}$  [12] has been assigned a configuration of  $\pi h_{9/2} \otimes \nu i_{13/2}^{-2} p_{3/2}^{-1}$  which arises from a coupling of the  $10^-$  ( $\pi h_{9/2} \otimes \nu i_{13/2}^{-1}$ ) with the two-neutron  $5^-$  ( $\nu i_{13/2}^{-1} p_{3/2}^{-1}$ ). Similarly, the  $16^-$  state, whose parity has been assigned in the present work, may have a configuration  $\pi h_{9/2} \otimes \nu i_{13/2}^{-1} f_{5/2}^{-2}$  arising from a coupling of the  $7^+$  ( $\pi h_{9/2} \otimes \nu f_{5/2}^{-1}$ ) with the two-neutron  $9^-$  ( $\nu i_{13/2}^{-1} f_{5/2}^{-1}$ ) configuration. The strong transitions between the band B1 and the  $16^-$  level indicate that they have similar configurations.

As already pointed out, the high-j  $\pi h_{9/2}$  and  $\pi i_{13/2}$  coupled to the  $\nu i_{13/2}^{-n}$  neutron holes play an important role in the generation of MR bands through the shears mechanism. Most of the MR bands in odd-A Pb isotopes have been understood in terms of the  $11^-$  two-proton configuration coupled to the  $i_{13/2}^{-n}$  neutron holes [7]. On the other hand, the MR bands in odd-A Bi isotopes are expected to have a configuration of  $\pi i_{13/2} h_{9/2}^2 \otimes \nu i_{13/2} \nu j$  and  $\pi i_{13/2} h_{9/2} s_{1/2} \otimes \nu i_{13/2} \nu j$ ; where  $j = (p_{3/2}, f_{5/2})$  [6, 10]. The MR band compilation [3] lists the assigned/suggested configurations for all the known MR bands.

We have plotted the angular momentum (I) vs.  $\hbar\omega$  bands B1, B2 and B3 in Fig. 6. We have also compared these plots with the other MR bands in the neighboring nuclides, namely  $^{197}\text{Bi}$  and  $^{197}\text{Pb}$  [6, 7]; some similarities are noticed which are helpful in fixing the configurations of these bands.

To assign possible configuration for the band B1, we note the similarities of this band with the neighboring odd-A Pb and Bi isotopes in Fig. 6 and the fact that the band head of this band decays strongly to the  $15^+$  isomer through a parity changing transition. As mentioned above, the configurations of the set of levels comprising of  $16^-$ ,  $17^+$ ,  $18^-$  and  $19^+$  (the band head of the band B1) states above the  $15^+$  isomer, may be considered as successive decoupling of neutrons (or protons) in positive and negative parity orbitals. The fact that these states lie close in energy, excitation of protons may be ruled out. Successive decoupling of neutrons in  $i_{13/2}$  and  $(p_{3/2}, f_{5/2})$  orbitals which lie close to each

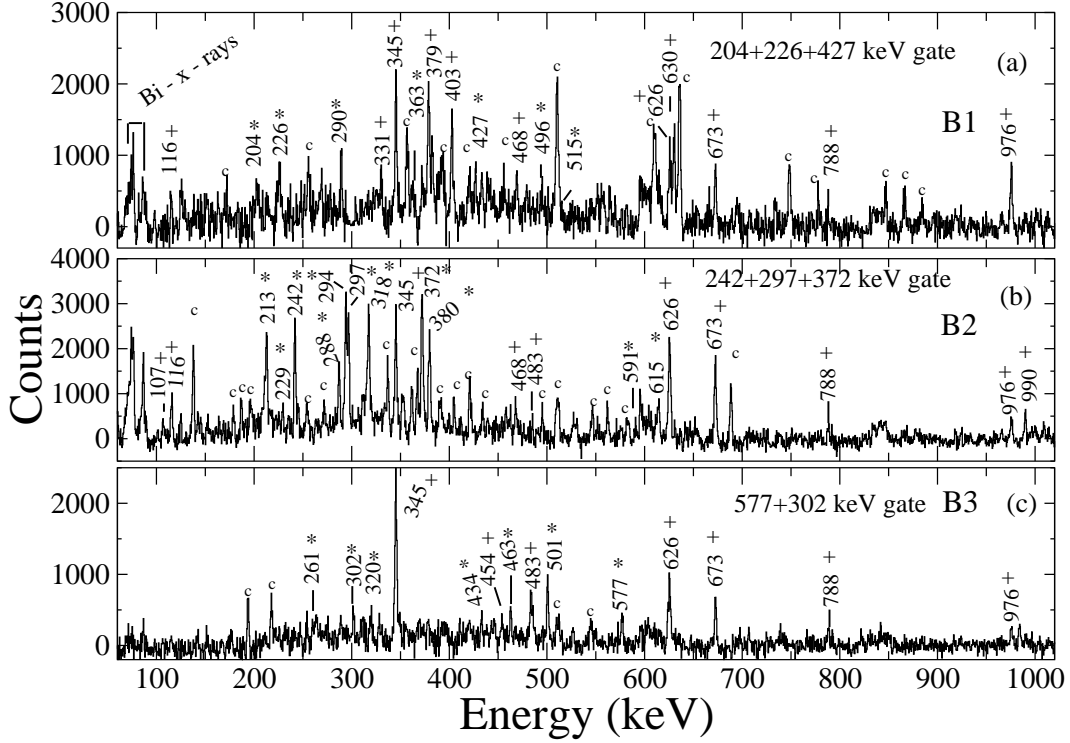


FIG. 5: Sum double gated spectra with gates on several in-band transitions belonging to bands B1 (a), B2 (b) and B3 (c) in  $^{198}\text{Bi}$ . The peaks marked by \* and + correspond to the in-band and the lower-lying transitions, respectively. Contaminated peaks are indicated by c.

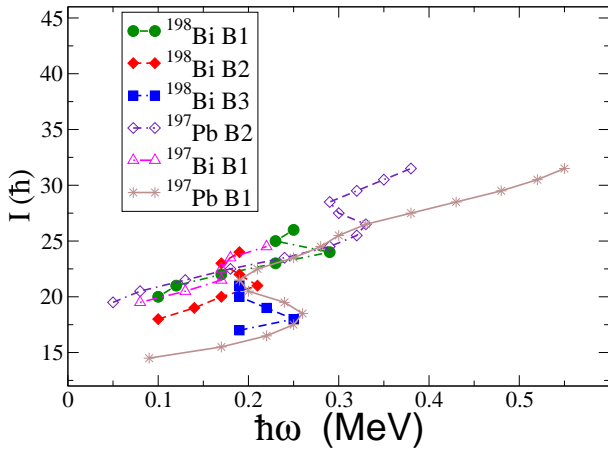


FIG. 6: (Color online)  $I$  (spin) vs.  $\hbar\omega$  (rotational frequency) plot for the MR bands in  $^{197}\text{Bi}$  [6],  $^{198}\text{Bi}$  and  $^{197}\text{Pb}$  [7].

other in energy, would be the most possible configuration of these states. Therefore, the configuration for the band B1 in  $^{198}\text{Bi}$  may be suggested as,  $\pi h_{9/2} \otimes \nu i_{13/2}^{-2} (p_{3/2}, f_{5/2})^{-3}$ , which is confirmed by the TAC calculations discussed later.

A backbending has been observed in this band above  $24\hbar$  of spin corresponding to a rotational frequency of  $\hbar\omega \sim 0.29$  MeV and the band becomes a 8-quasiparticle band. This band could not be extended much after the backbending so the details about the nature of the band after the alignment is not well known, but most likely, the configuration of the new band after the band crossing involves two more neutrons in the  $i_{13/2}$  orbital, which is again confirmed by the TAC calculations reported later.

Bands B2 and B3 lie at much lower excitation energies than the band B1 in  $^{198}\text{Bi}$  with bandhead spins and parities of  $17^-$  and  $(16^+)$ , respectively. The band B3 may be compared with the low-lying band B1 in  $^{197}\text{Pb}$ , which was assigned a configuration of two-proton  $11^-$  state coupled to a neutron hole in  $i_{13/2}$  [7] below the bandcrossing. It was argued in ref.[7] that additional two neutrons decouple at the bandcrossing frequency and this band continues with a three-neutron hole configuration coupled to the two-proton  $11^-$  state. The  $I$  vs.  $\hbar\omega$  plot of the band B1 in  $^{197}\text{Pb}$  is very similar to the band B3 in  $^{198}\text{Bi}$ . The backbending in these two bands take place also at the similar frequency. Considering the low-energy of the bandhead, the extra odd-proton in  $^{198}\text{Bi}$  may be in the  $h_{9/2}$  or-



bital. Therefore, the configuration of the band B3 in  $^{198}\text{Bi}$  below the band crossing is tentatively assigned as  $\pi i_{13/2} h_{9/2}^2 s_{1/2}^{-2} \otimes \nu i_{13/2}^{-1}$ . Two additional neutrons decouple quickly in this band and so, after the band crossing, it may have the configuration of  $\pi i_{13/2} h_{9/2}^2 s_{1/2}^{-2} \otimes \nu i_{13/2}^{-3}$ . However, detailed TAC calculations are unable to reproduce the features of this band. Further, the  $16^+$  level is tentative and its absence will change the nature of the completely. In all likelihood, it appears to be a purely shell model structure based on a multi-quasiparticle configuration. Similarly, considering the configurations reported in the neighboring odd-A nuclei and the  $j^\pi$  of the band, the bandhead configuration of the band B2 in  $^{198}\text{Bi}$  is proposed to be  $\pi h_{9/2} \otimes \nu i_{13/2}^{-3}$ . The TAC calculations reported in the following confirm this configuration assignment which also has a band-crossing from 4qp to 6qp configuration.

### A. Hybrid TAC Calculations

Tilted axis cranking (TAC) calculations have been performed to understand the band structures in  $^{198}\text{Bi}$ . The hybrid TAC model as described in ref. [3, 20, 21] and references there in, has been used for the calculations. The Hybrid version combines the best results of Woods-Saxon and Nilsson models. The single particle energies of the Woods-Saxon are taken and combined with the deformed part of the anisotropic harmonic oscillator. This has the advantage of using a realistic flat bottom potential along with the coupling between oscillator shells. Since pairing is an important parameter in these calculations, we have calculated proton and neutron pairing gap parameters  $\Delta_p$  and  $\Delta_n$  from the odd-even mass difference formula. Assuming that the pairing gets reduced for the excited configurations, we have attenuated these parameters by 20% and the proton and neutron gap parameters have been chosen to be 0.74 and 0.71 MeV, respectively.

#### 1. Band B1

Calculations have been performed for several possible proton and neutron configurations of this band considering a 6-quasiparticle bandhead with positive parity. Best results are obtained for the 6-qp configuration  $\pi h_{9/2} \otimes \nu i_{13/2}^{-2} (p_{3/2} f_{5/2})^{-3}$ . After the back-bending, it becomes a 8-quasiparticle configuration with an additional broken pair of neutrons in  $i_{13/2}$  orbital and the neutron configuration changes to  $\nu i_{13/2}^{-4} (p_{3/2} f_{5/2})^{-3}$ . The energy minimization as a function of deformation parameters for the 6-quasiparticle configuration gives self consistency at the

values of  $\epsilon_2 = -0.083$ ,  $\epsilon_4 = 0.003$  and  $\gamma = 6.9^\circ$  at tilted angle  $\theta = 57^\circ$ . The minimized values of deformation parameters for 8-qp configuration are  $\epsilon_2 = -0.085$ ,  $\epsilon_4 = 0.002$ ,  $\gamma = 1.1^\circ$  at tilted angle  $\theta = 64^\circ$ .

The spin vs. energy plot for this band is shown in Fig.7(a). It can be seen from this plot that there is an excellent agreement of the experimental data with the calculations for the 6qp configuration. The calculations have been extended for the 8qp configuration as well (shown as red dashed curve in Fig.7). It can be seen that the spin value of the crossing of the 6qp and 8qp bands is well reproduced in the calculations. Good agreement supports the assigned bandhead configuration of this band. The calculated values of  $B(M1)$  are shown in Fig.8(a). The decreasing trend of  $B(M1)$  values clearly indicates that the band B1 is an MR band. It may also be noted that a small and constant value of  $B(E2) = 0.07$  eb is obtained from the calculations for this band.

In Fig.9(a), we plot the spin vs.  $\hbar\omega$  values for this band and compare them with the calculated values. A reasonable agreement is observed before the band crossing. The calculated results after the bandcrossing deviates slightly from the experimental curve but the general trend is similar.

It may be noted that the possible configurations of this band are  $\pi h_{9/2}^2 s_{1/2} \otimes \nu i_{13/2}^{-3}$  and  $\pi i_{13/2} h_{9/2} s_{1/2} \otimes \nu i_{13/2}^{-2} (f_{5/2}, p_{3/2})^{-1}$ . The former configuration can be obtained from the coupling of two-proton  $5^-$  state with the  $10^-$  odd-odd valence-particle state with another two decoupled neutrons in  $i_{13/2}$  orbital and the later configuration is similar to those of band B2 in  $^{197}\text{Pb}$  and of the MR band in  $^{199}\text{Bi}$ . However, the TAC calculations for these bands are unable to reproduce the observed band for any of these configurations.

We may also note that the observation of a 6-qp MR band and its crossing with the 8-qp MR band is a very rare observation, and this is probably the second such observation in this region, only two other such observations are reported in  $^{108}\text{Cd}$  [3, 22, 23].

#### 2. Band B2

Since the band head of B2 is at a lower energy than B1 band, a 4-quasiparticle configuration of  $\pi h_{9/2} \otimes \nu i_{13/2}^{-3}$  has been assumed. After the back-bending, it becomes a 6-quasiparticle configuration by breaking an additional neutron pair in  $p_{3/2}$ . The 6qp configuration for this band will then be  $\pi h_{9/2} \otimes \nu i_{13/2}^{-3} p_{3/2}^{-2}$ . The minimization of the deformation parameters for 4qp configuration gives self consistency at the values  $\epsilon_2 = -0.085$ ,  $\epsilon_4 = 0.003$  and  $\gamma = 16.4^\circ$  at an average tilted angle of  $\theta = 70^\circ$ .

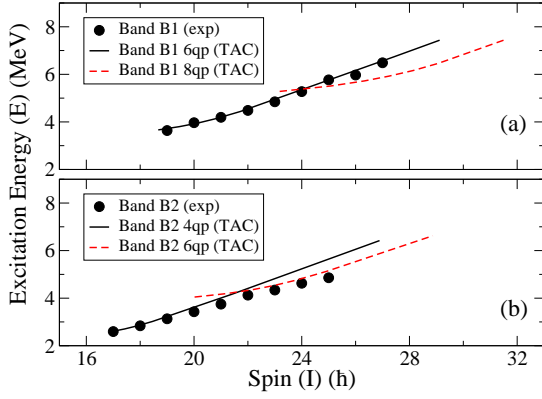


FIG. 7: (Color online) Spin vs. excitation energy plot for band B1 (a) and band B2 (b) in  $^{198}\text{Bi}$ . The filled circles are the experimental data while the solid and the broken lines are from the TAC calculations.

After the back-bending, the minimized values of deformation parameters for the 6qp configuration are  $\epsilon_2 = -0.090$ ,  $\epsilon_4 = 0.003$ ,  $\gamma = 4.5^\circ$  at an average tilted angle  $\theta = 65^\circ$ .

The spin vs. energy plot for this band has been shown in Fig.7(b). Again there is a very good agreement between the measured data and the calculated values. The band crossing is also well reproduced. After the bandcrossing at around  $22\hbar$ , the experimental values follow the calculations for 6qp configuration and thereby supporting the configurations assigned for this band before and after the bandcrossing.

The calculated  $B(M1)$  values for the 4qp and the 6qp configurations corresponding to the band B2 are shown in Fig.8(b). The decreasing values of  $B(M1)$  strongly supports the MR nature of this band as well. As the lifetime measurements were not possible in the present experiment, so it is not possible to compare the calculated  $B(M1)$  values with measured data. However, two cross-over transitions have been observed in this band from the  $20^-$  and  $21^-$  states, therefore the  $B(M1)/B(E2)$  ratios could be obtained for these two states from the intensities of the  $\Delta I = 2$  and the  $\Delta I = 1$  transitions (assuming mixing ratio  $\delta = 0$  for the MR bands). The  $B(M1)$  values can be obtained from these measured ratios using the calculated values of  $B(E2)$ . The  $B(M1)$  values for the two states obtained in this way are plotted in Fig.8(b) for comparison; an excellent agreement is observed. We also plot the spin ( $I$ ) vs.  $\hbar\omega$  for B2 band in Fig.9(b) and compare with the calculated values. Reasonable agreement is obtained before and after the crossing, confirming the 4-qp and 6-qp configurations before and after band crossing.

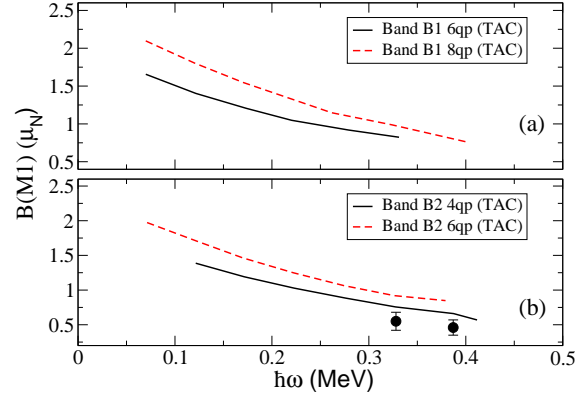


FIG. 8: (Color online)  $B(M1)$  values, obtained from the TAC calculations, as a function of rotational frequency  $\hbar\omega$  for band B1 (a) and band B2 (b) in  $^{198}\text{Bi}$ . The filled circles are obtained from the measured  $B(M1)/B(E2)$  ratios and using the  $B(E2)$  values from the TAC calculations for two of the states in band B2.

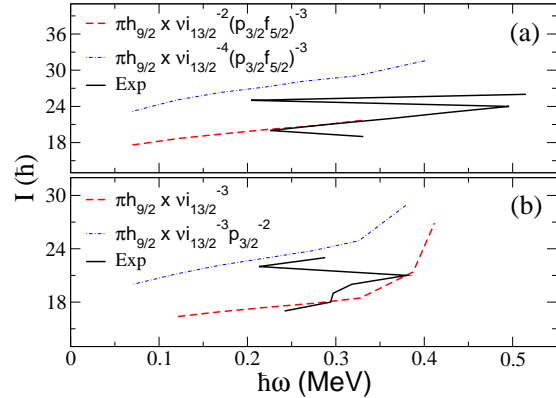


FIG. 9: (Color online) Spin ( $I$ ) vs. rotational frequency ( $\hbar\omega$ ) plot obtained from the TAC calculations for band B1 (a) and band B2 (b) in  $^{198}\text{Bi}$ . The calculated deformation parameters for band B1 are  $\epsilon_2 = -0.083$ ,  $\epsilon_4 = 0.003$ ,  $\gamma = 6.9^\circ$  for 6-qp configuration and  $\epsilon_2 = -0.085$ ,  $\epsilon_4 = 0.002$ ,  $\gamma = 1.1^\circ$  for 8-qp configuration. The same for band B2 are  $\epsilon_2 = -0.085$ ,  $\epsilon_4 = 0.003$ ,  $\gamma = 16.4^\circ$  for 4-qp configuration and  $\epsilon_2 = -0.089$ ,  $\epsilon_4 = 0.003$ ,  $\gamma = 4.5^\circ$  for 6-qp configuration. The experimental values are also shown.

## B. Semiclassical calculations for the bands B1 and B2

As the MR nature of the bands and their microscopic structure is well understood from the TAC calculations, the Bands B1 and B2 have been investigated in the frame work of a semiclassical model of magnetic rotation [1, 2, 24, 25] to get an idea about the particle-hole interaction strength. This calculation is based on a schematic model of the coupling of

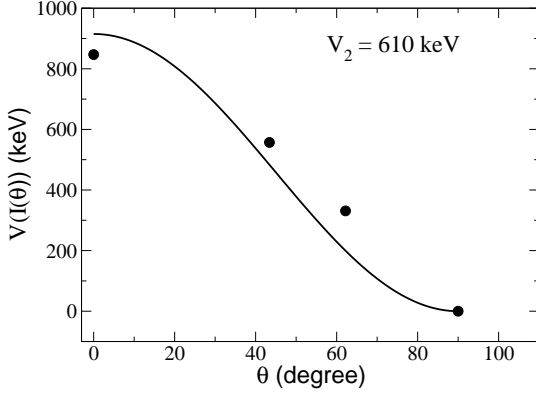


FIG. 10: The effective interaction between the angular momentum vectors,  $j_\pi$  and  $j_\nu$ , as a function of shears angle  $\theta$  for the band B1 in  $^{198}\text{Bi}$ .

two long  $j$  vectors, ( $j_\pi$  and  $j_\nu$ ), corresponding to the proton and neutron blades. This aims at extracting the information on the effective interaction between the nucleons which are involved in the shears mechanism. In this model, the shears angle ( $\theta$ ), between the two  $j$  vectors, is an important variable which can be derived using the equation

$$\cos\theta = \frac{I^2 - j_\pi^2 - j_\nu^2}{2 j_\pi j_\nu} \quad (3)$$

where,  $I$  is the total angular momentum. For the proposed configuration of  $\pi h_{9/2} \otimes \nu i_{13/2}^{-2} (p_{3/2} f_{5/2})^{-3}$  for band B1, the  $j_\pi$  and  $j_\nu$  values are  $4.5\hbar$  and  $17.5\hbar$ , respectively. Hence, the bandhead spin is calculated to be  $18.1\hbar$  assuming perpendicular coupling between  $j_\pi$  and  $j_\nu$ ; which is in reasonably good agreement with the observed bandhead. The maximum spin for this band can be calculated as  $22\hbar$  in this model. It can be seen from Fig.7(a) that the 6qp band crosses the 8qp band at around the similar values as obtained from the TAC calculations. Therefore, the semiclassical results are consistent with the TAC calculations.

According to the prescription of Macchiavelli *et al.* [24], the excitation energies of the states in shears bands correspond to the change in the potential energy because of the recoupling of the angular momenta of the shears. The excitation energies of the states in the band with respect to the band head energy can be written as:

$$V(I(\theta)) = E_I - E_b = (3/2)V_2 \cos^2\theta_I \quad (4)$$

where,  $E_I$  is the energy of the level with angular momentum  $I$ ,  $\theta_I$  is the corresponding shears angle as given in Eqn. 3,  $E_b$  is the bandhead energy and  $V_2$  is the strength of the interaction between the blades of the shears. Therefore,  $V_2$  can be calculated by using the experimentally observed energy levels of the

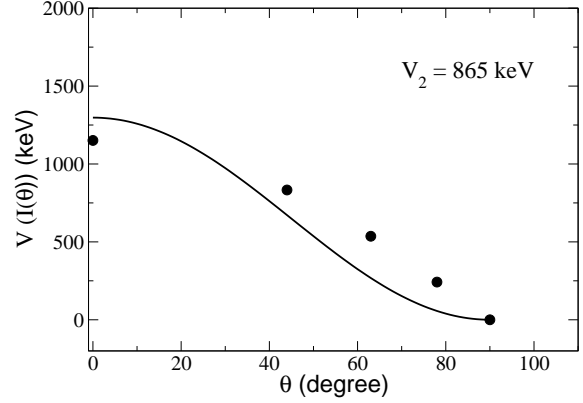


FIG. 11: Same as Fig.10 but for band B2 in  $^{198}\text{Bi}$ .

shears band.  $V(I(\theta))$ , obtained in this way for band B1, has been plotted as a function of  $\theta$  in Fig. 10.  $V_2$  has been extracted from this plot by a fit of equation 4. The fitted curve is shown as the solid line in Fig. 10. The extracted value of  $V_2$  comes out to be 610 keV, leading to the interaction strength per particle-hole pair ( $V_2^{p-h}$ ) as about 122 keV considering that all the five possible particle-hole pairs, in this configuration, are contributing to the shears mechanism. This is somewhat less compared to a typical value of  $V_2^{p-h} \sim 300$  keV observed in the Pb nuclei in this region [2]. This possibly indicates that all the particle-hole pairs may not be contributing equally to the shears mechanism. A value of  $V_2^{p-h} \sim 300$  keV is obtained if it is considered that the proton particles and neutron holes only in the high- $j$  ( $\pi h_{9/2}$  and  $\nu i_{13/2}$ ) orbitals are the dominant contributors to the shears mechanism.

Similarly, for the proposed configuration of band B2, the  $j_\pi$  and  $j_\nu$  values are  $4.5\hbar$  and  $16.5\hbar$ , respectively, and the calculated minimum (bandhead) and maximum spin values are  $17.1\hbar$  and  $21.0\hbar$ , respectively. The observed bandhead spin is again in very good agreement for this band also. The maximum spin corresponding to this configuration matches well with the observed backbending and with the spin value of  $21.6\hbar$  at which the 4qp and 6qp bands cross in the TAC calculations (see Fig.7(b)).

After the backbending, the band has a different configuration, so, in the subsequent calculations of  $V(I(\theta))$  the values of  $\theta$  were restricted up to the spin value of  $21\hbar$  as shown in Fig. 11. The extracted value of  $V_2$ , from this plot, comes out to be 865 keV. This leads to the interaction strength per particle-hole pair to be  $V_2^{p-h} = 288$  keV. This is in agreement with the typical values for this mass region. It may also be noted that the configuration of this band corresponds to proton particle and neutron holes in high- $j$   $\pi h_{9/2}$  and  $\nu i_{13/2}$  orbitals only

and hence, all the three possible particle-hole pairs contribute to the shears mechanism. Therefore, it supports the conjecture that the proton particles and neutron holes only in high-j orbitals have significant roles in forming MR bands by shears mechanism in this region.

#### IV. SUMMARY

We have investigated the high-spin structure of the odd-odd nucleus  $^{198}\text{Bi}$  by using the fusion-evaporation reaction with  $^{nat}\text{Re}$  target and 112.5 MeV beam of  $^{16}\text{O}$ . We have presented a new and much improved level scheme of this nucleus in this paper. The DCO ratio and the polarization asymmetry measurements have also been obtained to assign spins and parities of the levels. We have been able to identify three band structures, labelled as bands B1, B2 and B3, which lie at high excitation energies. On the basis of a comparison with similar bands in neighboring nuclei and the TAC calculations, we conclude that the bands B1 and B2 have a magnetic rotational character. One of the most significant findings of this work is the observation of the crossing of two MR bands in B1 as well as in B2 band. In the band B1, the lower part of the band has a 6-qp configuration  $\pi h_{9/2} \otimes \nu i_{13/2}^{-2} (p_{3/2} f_{5/2})^{-3}$ , which becomes a 8-qp configuration  $\pi h_{9/2} \otimes \nu i_{13/2}^{-4} (p_{3/2} f_{5/2})^{-3}$ , after the band crossing. Both the parts are MR in nature. Observation of such a crossing of two MR bands having large multi-quasiparticle configuration is a very rare finding. Similarly, the band B2 also undergoes a band crossing of two MR bands from a

4-qp configuration  $\pi h_{9/2} \otimes \nu i_{13/2}^{-3}$  to a 6-qp configuration  $\pi h_{9/2} \otimes \nu i_{13/2}^{-2} p_{3/2}^{-2}$ .

Although the measurement of BM(1) values are not available, the calculated B(M1) values perfectly fit the expected behaviour of MR bands. It is, however, strongly suggested that such measurements be carried out in future. We have also used the semi-classical model for the configurations assigned to bands B1 and B2 and have extracted the interaction strength of the particle-hole pairs, which fits into the previously observed trend. We conclude that the high-j proton particle and neutron hole pairs alone make the dominant contribution to the shears mechanism. We also conclude that the band B3 is a purely shell model structure and is a MR band.

#### V. ACKNOWLEDGEMENT

The authors gratefully acknowledge the effort of the pelletron operators at IUAC, New Delhi for providing a good quality of  $^{16}\text{O}$  beam. The help of Dr. P. Sugathan during the experiment is gratefully acknowledged. We thank all the members of INGA collaboration for setting up the array. Fruitful discussion regarding the polarization measurement with Prof. Maitreyee Saha Sarkar (Saha Institute of Nuclear Physics, Kolkata) is gratefully acknowledged. We also thank Prof. A.O. Macchiavelli (Lawrence Berkeley National Laboratory, USA) for valuable discussion. One of the authors (H. Pai) is thankful to Helmholtz International Center for FAIR for postdoctoral fellowship and Prof. Norbert Pietralla for several scientific discussion and motivation.

- 
- [1] H. Hübel, Prog. Part. Nucl. Phys. **54**, 1 (2005).  
 [2] R.M. Clark and A.O. Macchiavelli, Annu. Rev. Nucl. Part. Sci. **50**, 1 (2000).  
 [3] Amita, A.K. Jain and B. Singh, Atomic data and Nuclear data tables **74**, 283 (2000); <http://www.nndc.bnl.gov/publications/preprints/magn-dipole-16> (2006).  
 [4] G. Baldsiefen et al., Nucl. Phys. **A 574**, 521 (1994).  
 [5] A.K. Singh et al., Nucl. Phys. **A 707**, 3 (2002).  
 [6] G.K. Mabala et al., Eur. Phys. J. **A 25**, 49 (2005).  
 [7] A. Görgen et al., Nucl. Phys. **A 683**, 108 (2001).  
 [8] H. Pai et al., Phys. Rev. **C 85** 064313 (2012).  
 [9] G. Zwartz et al., J. Phys. G: Nucl. Part. Phys. **26** 849 (2000).  
 [10] P.J. Dagnall et al., J. Phys. G: Nucl. Part. Phys. **20** 1591 (1994).  
 [11] U. Hagemann et al., Nucl. Phys. **A 197** 111 (1972).  
 [12] X.H. Zhou et al., Phys. Rev. **C 54** 2948 (1996).  
 [13] S. Muralithar et al., Nucl. Instrum. Methods Phys. Res. **A 622**, 281 (2010).  
 [14] D. C. Radford, Nucl. Instrum. Methods Phys. Res. **A 361**, 297 (1995).  
 [15] A. Krämer-Flecken, et al., Nucl. Instrum. Methods Phys. Res. **A 275**, 333 (1989).  
 [16] E. Sandoval et al., Computer Phys. Comm **11**, 75 (1976).  
 [17] K. Starosta et al., Nucl. Instrum. Meth. Phys. Res. **A 423**, 16 (1999).  
 [18] Ch. Droste et al., Nucl. Instrum. Meth. Phys. Res. **A 378**, 518 (1996).  
 [19] R. Palit et al., Pramana **54**, 347 (2000).  
 [20] V. I. Dimitrov, F. Dönau, and S. Frauendorf, Phys. Rev. **C 62**, 024315 (2000).  
 [21] Amita, A.K. Jain, V.I. Dimitrov and S.G. Frauendorf, Phys. Rev. **C 64**, 034308 (2001).  
 [22] N. S. Kelsall et al., Phys. Rev. **C 61**, 011301(R)(1999).  
 [23] A. Görgen et al., Nucl. Phys. **A 683** 108 (2001).

- [24] A.O. Macchiavelli et al., Phys. Rev. C **57**, R1073 (1998).
- [25] A.O. Macchiavelli et al., Phys. Rev. C **58**, R621